ROR2 drives right ventricular heart failure via disruption of proteostasis

Hali Hartman B.S.[1], Genevieve Uy B.S.[1], Keita Uchida Ph.D.[2], Emily A. Scarborough Ph.D.[2], Yifan Yang M.S.[3], Eric Barr B.S.[1,3], Spencer Williams B.S.[1], Ryan T. Santilli B.S.[1], Sanam L. Kavari B.S.i[3], Jeff Brandimarto M.S.[3], Li Li B.S.[2], Ling Lai M.D.[3], Joanna Griffin[3], Nora Yucel Ph.D.[3], Swapnil Shewale Ph.D.[3], Hari Rajagopal[1], Deborah M. Eaton Ph.D.[3], Tanis Dorwart B.S.[4], Kenneth C. Bedi Jr B.S.[3], Crystal S. Conn Ph.D.[4], Kenneth B. Margulies M.D.[3], Benjamin Prosser Ph.D.[2], *Zoltan Arany M.D., Ph.D.[2,3], *Jonathan J. Edwards M.D.[1,3]

[1]Cardiovascular Institute, Children's Hospital of Philadelphia, Philadelphia, PA, USA

[2]Department of Physiology, Pennsylvania Muscle Institute, Perelman School of Medicine, University of Pennsylvania, Philadelphia, PA, USA

[3]Cardiovascular Institute, Perelman School of Medicine, University of Pennsylvania, Philadelphia, PA, USA

[4]Department of Radiation Oncology, Perelman School of Medicine, University of Pennsylvania, Philadelphia, PA, USA

*Contributed equally

Short Title: ROR2 drives right ventricular heart failure

Correspondence to:
Jonathan Edwards, MD
University of Pennsylvania
Cardiovascular Institute
3401 Civic Center Blvd
Smilow Center for Translational Research, Room 11-114
Philadelphia, PA 19104
EdwardsJ6@chop.edu

Zoltan Arany, MD, PhD
University of Pennsylvania
Cardiovascular Institute
3401 Civic Center Blvd
Smilow Center for Translational Research, Room 11-106
Philadelphia, PA 19104
zarany@pennmedicine.upenn.edu

Word Count: 4993 (limit 5000)

Abstract

Background: No therapies exist to reverse right ventricular failure (RVF), and the molecular mechanisms that drive RVF remain under studied. We recently reported that the developmentally restricted noncanonical WNT receptor ROR2 is upregulated in human RVF in proportion to severity of disease. Here we test the mechanistic role of ROR2 in RVF pathogenesis.

Methods: ROR2 was overexpressed or knocked down in neonatal rat ventricular myocytes (NRVMs) and then characterized using confocal microscopy, RNAseq, proteomics, proteostatic functional assays, and pacing to assess contractile properties. The impact of cardiac ROR2 expression was evaluated in mice by AAV9-mediated overexpression and by AAV9-mediated delivery of shRNA to knockdown ROR2 in a pulmonary artery banded pressure overload model of RVF. ROR2-modified mice were evaluated by echocardiography, histology, and RV protein synthesis and proteasome capacity.

Results: In NRVMs, we find that ROR2 profoundly dysregulates the coordination between protein translation and folding. This imbalance leads to excess protein clearance by the ubiquitin proteasome system (UPS) with dramatic impacts on sarcomere and cytoskeletal structure and function. Inhibiting the UPS or restoring chaperone expression is sufficient to partially rescue ROR2-induced structural and contractile deficits in cardiomyocytes. In mice, forced cardiac ROR2 expression is sufficient to disrupt proteostasis and drive RVF, while conversely ROR2 knockdown partially rescues proteostasis and RV structure and function in a pressure overload model of RVF.

Conclusions: In sum, ROR2 is a key driver of RVF pathogenesis through proteostatic disruption and, thus, provides a promising target to treat RVF.

62 **Introduction**

63 Right ventricular failure (RVF) is a widespread problem for which there are no proven therapies.
64 Nearly half of patients with left ventricular failure (LVF) develop RVF, and RVF doubles their risk
65 of death.[1,2] RVF is also the leading cause of hospital admission and death in pulmonary
66 hypertension.[3-5] For LVF, there are several therapies that can reduce patient morbidity and
67 mortality.[6] In contrast, no therapies have proven efficacious for patients with RVF, and in fact,
68 some medications that benefit LVF led to worse outcomes.[7-13] RVF thus fundamentally differs
69 from LVF, and finding new therapies for RVF will require a deeper understanding of targetable
70 molecular drivers of RVF.[14,15]

71

72 We recently analyzed a large cohort of human hearts from patients transplanted for dilated or
73 ischemic cardiomyopathy, and discovered that the noncanonical WNT receptor ROR2—usually
74 developmentally restricted—is robustly upregulated in failing RVs, and its expression correlated
75 with RVF severity.[16] ROR2 is essential for the development of multiple organ systems, including
76 the heart.[17] *Ror2* knockout caused ventricular septal defects in mice, while loss of *Ror1* did not
77 impact heart development.[17-19] However, combined *Ror1/Ror2* double knockout caused more
78 severe developmental pathologies including complex conotruncal defects and ventricular
79 noncompaction. The mechanistic role of ROR2 in RVF, however, has not been explored.

80 We investigated whether ROR2 induction contributes to RVF and identified a previously
81 unrecognized role for ROR2 in regulating cardiomyocyte proteostasis. ROR2 induction disrupts
82 the balance between protein synthesis and folding capacity and increases ubiquitin proteasome
83 system (UPS)-mediated protein degradation. This UPS response is either inadequate or
84 excessive to the point being maladaptive, further contributing to RVF pathogenesis. In a mouse

model of RVF, preventing ROR2 induction ameliorated both RV proteostatic disruption and RVF. These findings indicate that targeting ROR2-driven proteostatic disruption may offer a new therapeutic approach for RVF.

Methods

Detailed methods are provided in the Supplemental Material. Source data supporting the findings and displayed in main figures and supplemental figures are also included in the Supplemental Material. RNAsequencing data generated for this study was deposited in the Gene Expression Omnibus under the accession number GSE278627. The mass spectrometry proteomics data have been deposited to the ProteomeXchange Consortium via the PRIDE partner repository with the dataset identifier PXD05655.[20]

Animal Studies

All animal work was performed under University of Pennsylvania Institutional Animal Care and Use Committee approved protocols (#805255, #805309, and #807751). Neonatal rat ventricular myocytes (NRVMs) were isolated from 1-2 day old Sprague Dawley rats after obtaining pregnant rats from Charles River Laboratory and maintained in culture as previously described.[21] C57BL/6J mice obtained from Jackson Laboratory were used for all mouse experiments studies.

Human Studies

Procurement of all human RV myocardial tissue was performed in accordance with protocols approved by the University of Pennsylvania Institutional Review Board (approval 802781) and the Gift-of-Life Donor Program, Philadelphia, PA. Prospective informed consent for research

107 use of surgically explanted tissue was obtained from the transplant recipients or from the next-
108 of-kin in the case of deceased organ donors, as previously described.[22]

109

110 **Statistical Analyses**

111 RNAseq and proteomics data were analyzed in RStudio using the voom function from the
112 Limma package (version 3.56.1) to transform and normalize the data, and the toptable function
113 to output the differential analysis result. Two group and three group statistical comparisons were
114 performed in GraphPad Prism v10 using T-test/Mann Whitney U or One-Way ANOVA/Kruskal-
115 Wallis/Two-Way ANOVA based on normality and number of independent variables.

116

117 **Results**

118 Cardiomyocyte ROR2 expression is developmentally restricted and reactivated in RV failure

119 ROR2 is necessary for heart development and its expression is broadly absent in healthy adult
120 tissues, but the temporal nature for its loss and its histologic pattern in the early postnatal heart
121 has not been well characterized.[23] By qPCR and western blot, we observe maturity dependent
122 loss of ROR2 with about 70% reduction in ventricular ROR2 from P2 to P7 and near loss of
123 ROR2 by P21 (**Fig. 1a, Supplementary Fig. 1a/b**). Myocardial ROR2 at birth is observed
124 predominantly in cardiomyocytes with localization to the cell membrane and nucleus (**Fig 1b**
125 and **Supplementary Fig. 1c**). With postnatal maturation, ROR2 is minimally retained and
126 mostly observed in the atria and subepicardium (**Fig 1a** and **Supplementary Fig. 1c/d**),
127 consistent with prior single nuclear RNAseq datasets.[24,25] Nuclear localizing ROR2 has been
128 observed in some cancers, which has been linked to worse outcomes. Therefore, we further

129 evaluated ROR2 localization using a protein fractionation method that separates nuclear
130 depleted cytoplasmic proteins ("NCD") from a nuclear enriched fraction that also contains
131 cytoskeleton proteins ("NCE") (**Supplementary Fig. 1e/f**).[26-28] We found most ROR2 localized
132 to the NCD fraction, but the temporal loss of ROR2 is comparable across total, NCD, and NCE
133 fractions.

134

135 We previously found that ROR2 is re-expressed in human RVF in a severity dependent manner,
136 localizing to both cardiomyocytes and fibroblasts.[16] This pattern differs from a prior study in
137 mouse pressure overload LVF where ROR2 induction was restricted to noncardiomyocytes, so
138 we next tested if and where ROR2 is reactivated in the failing mouse RV.[29] To that end, we
139 used a pulmonary artery band (PAB) pressure overload model to generate RVF. With an
140 average pressure gradient of ~60-70mmHg, PAB mice developed clear markers of pathologic
141 RV remodeling and RVF with increased RV mass, and echocardiographic RV hypertrophy,
142 dilation, systolic dysfunction, and tricuspid insufficiency (**Fig. 1c-f** and **Supplementary Table 1**).
143 PAB also caused RV wall thickening and diffuse RV fibrosis by histology (**Fig. 1g**). PAB RVs
144 also demonstrate increased expression of the classic heart failure markers fetal myosin heavy
145 chain protein MYH7 and the natriuretic peptide transcript *Nppb* (**Fig. 1h/i**). In parallel, ROR2
146 was induced ~5-fold in the NCD fraction and more than 30-fold in the NCE fraction. (**Fig. 1j/k**).
147 Thus, the normally developmentally restricted ROR2 is robustly reexpressed in mouse RVF (**Fig**
148 **1l**). Interestingly, NCE ROR2 strongly correlated to RV functional and structural changes in PAB
149 including the severity of RV dilation (r=0.66), TAPSE (r= -0.69), and fractional area change (r= -
150 0.60) (all $p<0.05$, **Supplementary Table 1**). In contrast, NCD ROR2 showed no significant
151 correlation to any of these RV functional or structural parameters. Induced ROR2 localized to
152 both cardiomyocytes and fibroblasts in the PAB RV by immunohistochemistry and RNAscope.
153 ROR2 protein in cardiomyocytes localized to the cytoplasm, membrane, and nucleus (**Fig. 1m**)

154 similar to ~P2-P7 mouse RV and consistent with the NCD/NCE fractionation. This was also
155 consistent with our previous findings in human RVF immunohistochemistry and further
156 supported by complementary immunohistochemistry and RNAscope of human RVs in this study
157 (**Supplementary Fig. 2a/b).** We conclude that ROR2 expression, particularly the NCE fraction,
158 is strongly induced in mouse RVF and increases in proportion to RVF severity.

159

160 <u>ROR2 regulates cardiomyocyte morphology</u>

161 Since little is known about the role of ROR2 in cardiomyocytes, we directly tested the impact of
162 ROR2 induction and loss using NRVMs. We cultured cells on patterned substrates to promote
163 sarcomere alignment, allowing more robust structural characterization. We overexpressed
164 human ROR2 ($ROR2^{OE}$) or knocked down native *Ror2* by shRNA ($ROR2^{KD}$) using adenovirus
165 with a GFP reporter (**Fig. 2a/b**). Adeno-GFP alone was used as a control. $ROR2^{OE}$ and $ROR2^{KD}$
166 caused dichotomous morphologic changes. $ROR2^{OE}$ NRVMs had fragmented sarcomeres and
167 were significantly smaller, driven by reduction in the longitudinal major axis, with a rounded
168 appearance and smaller aspect ratio (major/minor axis) (**Fig. 2c-e**). In contrast, $ROR2^{KD}$
169 NRVMs were slightly larger without affecting the aspect ratio. We also observed opposing
170 effects on cell-cell junctions with $ROR2^{KD}$ increasing and $ROR2^{OE}$ decreasing peripheral
171 enrichment of the intercalated disc (ICD) localizing proteins α-actinin, β-catenin, and Cx43 (**Fig.
172 2f-h** and **Supplementary Fig. 3a**). Total Cx43 and α-actinin staining intensity and protein
173 expression by western blot increased in $ROR2^{OE}$ NRVMs, while β-catenin levels were stable,
174 indicating that reduced peripheral staining represents redistribution of the proteins rather than
175 loss (**Fig 2i-l)**. Thus, ROR2 regulates gross cardiomyocyte morphology and both abundance
176 and peripheral localization of ICD/junction proteins.

177

178 ROR2 affects cardiomyocyte ubiquitin-proteasome system, protein folding, and synthesis

179 We used RNAseq of ROR2^{OE} and ROR2^{KD} NRVMs to investigate potential mechanisms for
180 these NRVM structural phenotypes (**Fig. 3a** and Supplementary Data 4). We observed that β-
181 catenin responsive transcriptional targets were not significantly impacted, indicating no
182 significant role for canonical WNT signaling (**Supplementary Table 2** and **Data 5**). Instead,
183 gene-set enrichment analysis revealed changes in protein turnover gene programs, which
184 included upregulation ubiquitin ligase activity genes and downregulation for ubiquitin-dependent
185 protein catabolism genes in ROR2^{OE} (**Fig. 3b**). Interestingly, at the protein level, total ubiquitin
186 was significantly decreased in ROR2^{OE} but unchanged in ROR2^{KD} (**Fig 3c/d**). We tested
187 whether the reduction of ubiquitinated proteins in ROR2^{OE} NRVMs was driven by increased
188 turnover or decreased ubiquitination by blocking clearance of ubiquitinated proteins using the
189 competitive proteasome inhibitor MG132. As expected, MG132 increased accumulation of total
190 ubiquitin across all groups, with ROR2^{OE} NRVMs demonstrating significantly greater
191 accumulation of proteasome directing K48 ubiquitin (**Fig 3e/f** and **Supplementary Fig 3b**).
192 Interestingly, ROR2^{KD} demonstrated lower basal K48 ubiquitin with intact accumulation of both
193 total and K48-linked ubiquitin. We next measured maximal proteasome capacity by incubating
194 cell lysates with Suc-LLVY-AMC—a fluorescent reporter containing a peptide substrate of the
195 chymotrypsin-like proteasome subunit (PSMB5). ROR2^{OE} increased PSMB5 maximal capacity
196 at 0 and 3.5μM ATP, and trended towards an increase at 7μM ATP, without affecting total
197 PSMB5 expression (**Fig 3g** and **Supplementary Fig 3c)**. Whereas, ROR2^{KD} did not impact
198 PSMB5 expression or maximal capacity, mirroring the intact accumulation of ubiquitin. Thus,
199 these data indicate that ROR2 expression significantly alters the UPS, with high ROR2
200 promoting K48 ubiquitination and proteasome-mediated turnover while low ROR2 decreases

201 K48 ubiquitination without affecting proteasome capacity, indicating additional levels of
202 proteostatic regulation.

203

204 In addition to UPS related transcriptional changes, the two HSP70 paralogs *Hspa1a* and
205 *Hspa1b* exhibited the highest magnitude reduction in ROR2^{OE} (log_2FC <-4.7, adj p =0.059,
206 both). Multiple other chaperones were also trending as significantly downregulated (adj p <0.1)
207 including *Hsph1/Hspa4* (HSP105/110), *Hsp90aa1/ab1*, *Dnajb1/a1 (*HSP40), and *Cryab* (**Fig 3a)**.
208 At the protein level, most tested chaperones including HSP70 were significantly increased in
209 ROR2^{KD}. Whereas, in ROR2^{OE}, HSP70 was significantly decreased, and other tested
210 chaperones were unchanged (**Fig. 3c/h** and **Supplementary Fig 3d**). To directly measure
211 protein folding capacity, we used a luciferase refolding assay in which heat-shocked
212 recombinant luciferase is allowed to refold in cell lysates supplemented with protease inhibitor
213 and then interrogated by its ability to cleave luciferin thereby generating light (**Fig. 3i**).
214 Consistent with reduced HSP70 expression, refolding of heat-shocked recombinant luciferase
215 was significantly impaired in ROR2^{OE} lysates. Despite globally increased chaperone expression,
216 luciferase refolding was unaffected in ROR2^{KD}. This result may be explained by GFP control
217 lysates exceeding a minimum HSP70 threshold to sufficiently refold heat shocked luciferase or
218 by ROR2^{KD} also increasing HSP105/110, which can lead to premature release of protein
219 substrates that diminishes refolding efficiency (**Supplementary Fig 3c**).[30]

220

221 Given the ROR2-responsive effects on protein folding and UPS, we next tested whether other
222 aspects of protein production or stability may also be disrupted. We quantified global protein
223 synthesis rates by using the tyrosyl tRNA analogue puromycin and radiolabeled ^{35}S-Met to label

224 newly synthesized proteins. By puromycin labeling, ROR2^{OE} resulted in ~2-3-fold increase in
225 protein synthesis and ROR2^{KD} modestly decreased translation (**Fig. 3j/k)**. ^{35}S-Met labeling
226 revealed similar results with ~1.5-fold increase in ROR2^{OE} and ~0.6-fold reduction in ROR2^{KD}
227 (**Supplementary Fig. 3e**). ROR2-driven effects on protein synthesis were unlikely a secondary
228 effect of altered chaperone expression, as HSP70 overexpression (HSP70^{OE}) did not reverse
229 the differential translation rates or ubiquitin levels (**Supplementary Fig. 3f/g**). However, given
230 the observed differences in protein synthesis, folding, and proteasome capacity with ROR2
231 modulation, we considered whether the stability of newly synthesized proteins differed across
232 groups. To that end, we performed a pulse chase experiment consisting of a 1 hour of
233 puromycin labeling followed by a 1hr incubation with cycloheximide to block further protein
234 synthesis with or without MG132 or HSP70^{OE}. We found that turnover of newly synthesized
235 proteins was ~2-fold higher in ROR2^{OE} (~50% vs. 25%) compared to controls, and ROR2^{KD}
236 demonstrated decreased turnover (<10%) indicating increased protein stability. Strikingly,
237 MG132 and HSP70^{OE} equivalently increased the stability of newly synthesized proteins ROR2^{OE}
238 and control NRVMs, but these only reached statistical significance for ROR2^{OE}. We also tested
239 protein stability using the constitutive UPS substrate GFPμ, which required generating ROR2
240 modified NRVMs lacking a GFP reporter (**Supplementary Fig. 3h-k**). By microscopy, flow
241 cytometry, and western blot, GFPμ was consistently lowest in ROR2^{OE} and highest in ROR2^{KD},
242 even in the presence of MG132. Using bafilomycin, we excluded the possibility that autophagy
243 contributed to GFPμ clearance independently or in combination with proteasome inhibition. Of
244 note, although GFPμ remained lowest in ROR2^{OE}, the relative increase of GFPμ by MG132 was
245 most pronounced in ROR2^{OE}. Comparing these results with the puromycin pulse chase
246 experiments highlights the importance of considering total protein synthesis rates and baseline
247 GFPμ levels when interpreting GFPμ flux. These results also suggest that ROR2 increases
248 protein synthesis in a biologically selective manner. Taken together, these data show that ROR2

249 profoundly disrupts cardiomyocyte proteostasis by promoting protein synthesis while
250 simultaneously suppressing folding capacity, priming NRVMs to clear proteins through the UPS.

251

252 ROR2 impairs cardiomyocyte structure and function via Proteostatic Disruption

253 Next, to determine if changes in the proteostatic balance were responsible for the NRVM
254 morphologic changes observed with $ROR2^{OE}$, we repeated the morphology evaluations with a
255 24-hour incubation of 1 μM MG132. Proteasome inhibition significantly abrogated the impact of
256 $ROR2^{OE}$ on NRVM morphology with improvement in the sarcomere pattern, aspect ratio, and
257 peripheral localization of α-actinin localization (**Fig. 4a-c** and **Supplementary Fig. 3m**). We also
258 tested the impact of increased folding capacity by $HSP70^{OE}$, which similarly improved $ROR2^{OE}$
259 NRVM morphology by increasing cell area and aspect ratio, but not to the extent of proteasome
260 inhibition (**Fig. 4d-f**).

261

262 We next tested the impact of ROR2 modulation on cardiomyocyte contractile properties. Using
263 an IonOptix Cytocypher pacing apparatus, we found that $ROR2^{OE}$ significantly slowed
264 contractile and relaxation kinetics, and that $ROR2^{KD}$ accelerated relaxation (**Fig. 4g-k**).
265 Strikingly, $HSP70^{OE}$ accelerated contraction and relaxation kinetics in both $ROR2^{OE}$ and control
266 NRVMs to match $ROR2^{KD}$ (**Fig. 4g-k**). Taken together, these data demonstrate that disruptions
267 in proteostatic balance—including UPS-mediated turnover and folding capacity—are primary
268 mechanistic mediators of ROR2-responsive effects on NRVM morphology and function.

269

270 ROR2 regulates the cardiomyocyte proteome

271 In light of the profound effects of ROR2 on proteostatic balance and evidence that ROR2
272 impacts protein synthesis and turnover in a selective manner, we next sought to characterize
273 the interaction between ROR2 expression and proteasome inhibition on the global proteome
274 (**Fig. 5a-c**). By principal component analysis plot, we observed tight clustering by groups with
275 PC1 correlating to MG132 and PC2 correlating to $ROR2^{OE}$ effects (**Fig 5c**). Accordingly,
276 $ROR2^{OE}$ dramatically altered the NRVM proteome, which was broadly reversed by proteasome
277 inhibition (**Fig 5a/b**). We considered whether intrinsic protein characteristics contributed to
278 $ROR2^{OE}$-mediated effects on the global NRVM proteome. Using a comprehensive dataset of
279 protein half-lives in mouse fibroblasts and known molecular masses as indicators of stability and
280 complexity, we found that upregulated proteins (adj $P<0.05$) were smaller and exhibited longer
281 predicted half-lives compared to downregulated proteins (65.8 kDa vs. 87.5 kDa and 134 vs. 55
282 hours, $p<0.0001$, both, **Supplementary Fig a/b**).[31] However, the magnitude of up- or down-
283 regulation did not correlate directly to protein mass or predicted half-lives, suggesting additional
284 levels of regulation **(Supplementary Fig 4c-f**). $ROR2^{OE}$ did not significantly affect the
285 expression of proteasome subunits, consistent with similar PSMB5 levels by western blot as
286 noted above. In contrast, we found $ROR2^{OE}$ significantly altered E3 ubiquitin ligase expression
287 (20 upregulated and 26 downregulated), some of which was reversed by proteasome inhibition,
288 indicating substantial protein substrate-specificity for ROR2-driven UPS-mediated clearance
289 (**Fig**. **5d/e**, Supplementary Data 20 and 21). These included upregulation of OZZ-E3 (*Neurl2*)—
290 a ubiquitin ligase that targets β-catenin specifically at the intercalated disc—and ITCH—which
291 targets the non-canonical WNT signaling protein DVL (**Fig 5d**)**.** PDZRN3, an E3 ligase that was
292 recently identified as a likely indirect ROR2 phosphorylation target and which plays a role in
293 postnatal sarcomerogenesis and ICD formation, was also significantly reduced.[32,33] In contrast,
294 we observed no changes in the components of the E3 ligase complex $SCF^{\beta\text{-}TRCP}$ that targets the

295 transcriptional pool of β-catenin, which is consistent with no substantial changes in canonical
296 WNT signaling by RNAseq (**Supplementary Fig. 4a**).

297

298 Pathway enrichment analysis revealed that proteins which were upregulated by ROR2^{OE} were
299 enriched for multiple biological processes including triglyceride biosynthesis, extracellular matrix
300 proteins, integrin-mediated signaling, heart contraction, and response to insulin. Notable
301 upregulated proteins included myogenic differentiation factors VGLL3 and MEF2A—consistent
302 with an immature state—and regulators of calcium homeostasis PLN, CAMK2D, and
303 CAMK2A—which may contribute to altered contractile kinetics. Moreover, in the setting of
304 junctional proteins being mislocalized in ROR2^{OE} by microscopy, the increase in integrin
305 associated proteins may reflect a compensatory attempt to establish cell-cell junctions.
306 Interestingly, of 426 proteins with at least logFC >0.5 upregulation (adj $p<0.05$), 60% were
307 significantly decreased by proteasome inhibition compared to 2% that were further increased.
308 Downregulated proteins were enriched for regulators of proline hydroxylation, sarcomere and
309 actin filament organization, supramolecular organization, and inhibitors of apoptosis (**Fig. 5f**).
310 Mirroring the behavior of upregulated proteins, 60% of the 559 downregulated proteins (logFC <
311 -0.5, adj $p<0.05$) were significantly increased by MG132 with 6% demonstrating further
312 reduction. Importantly, reversal of downregulated proteins included many actin cytoskeleton and
313 sarcomere associated proteins including: TPM1/2/3, XIRP1/2, MYOZ2, LMOD2, FLNC, NRAP,
314 and TNNT2 (**Fig. 5g** and **Supplementary Fig. h/i**). Thus, we conclude that ROR2-mediated
315 disruption of the cardiomyocyte proteome impinges on cardiomyocyte differentiation, structural,
316 functional, and adhesion proteins, that are largely dependent on altered UPS activity.

317

318 Cardiac ROR2 expression causes RV failure and proteostatic disruption

319 Given the marked effects of ROR2^{OE} in cardiomyocytes in cell culture, we next sought to test
320 the effect of ROR2 expression in the RV *in vivo*. To this end, we generated cardiac ROR2^{OE}
321 mice using AAV9 to deliver HA-tagged ROR2 versus GFP in 4-week-old male and female mice
322 (**Fig. 5a**). At 8 weeks after injection, we observed robust RV and LV ROR2 expression, which
323 localized to the cardiomyocyte membrane and cytoplasm (**Fig. 6b, Supplementary Figs. 1a**
324 **and 5a**). ROR2^{OE} led to significant RV hypertrophy in male mice, marked by an increase in RV
325 mass, RV wall area, and RV cardiomyocyte cross-sectional area by minimum Feret Diameter
326 (**Fig. 6b-h**). Echocardiography (n=8/group, 50% male) revealed biventricular dilation and
327 systolic dysfunction in male ROR2^{OE} mice (**Fig. 6i-l** and **Supplementary Table 3**). Cardiac
328 catheterization revealed a male-specific increase in RV end diastolic pressure (**Fig. 6m**).
329 ROR2^{OE} male mice also exhibited induction of *Nppb* mRNA and fetal MYH7 **(Fig. 6n/o**) without
330 causing an increase in fibrosis (**Fig. 6p**). The cardiac dysfunction seen in male ROR2^{OE} mice
331 was accompanied by proteostatic disruptions similar to those seen in NRVMs including lower
332 *Hspa1b* mRNA, decreased cardiomyocyte ubiquitin staining, increased protein synthesis, and
333 increased proteasome capacity **(Fig. 6q-u** and **Supplementary Table 4**). We also observed
334 reduced peripheral β-catenin in RV cardiomyocytes consistent with disrupted cell-cell junctions
335 that mirror effects seen in NRVMs (**Supplementary Fig. 5b/c**). We conclude that ROR2
336 expression is sufficient to drive RV failure *in vivo* in male mice, concomitant with disruption of
337 proteostasis, whereas female ROR2^{OE} mice were generally much less affected.

338

339 Suppression of ROR2 induction in RV pressure overload abrogates RV failure and proteostatic
340 disruption

341 The results above demonstrated that ROR2 expression was sufficient to cause RV dysfunction
342 and disrupt proteostasis. We next sought to test if ROR2 expression was necessary for RVF in
343 the PAB mouse model and its role in proteostasis. We first evaluated the proteostatic signature
344 of PAB-induced RVF, noting that PAB increased RV protein synthesis, HSP70, and total
345 ubiquitin—with K48 ubiquitin and PSMB5 increased in the NCE fraction—and proteasome
346 capacity (**Fig. 7a-g** and **Supplementary Table 5**). Thus, the PAB RVF mouse model
347 demonstrates clear proteostatic disruption with an increase in both protein synthesis and UPS-
348 mediated turnover, to some extent analogous to that found with $ROR2^{OE}$. Next, to determine if
349 ROR2 induction in PAB contributes to RVF and proteostatic disruption, we injected male mice
350 with AAV9 to deliver *shRor2* (PAB^{shRor2}, n = 15) or scrambled shRNA (PAB^{shScr}, n=15) prior to
351 PAB. Since ROR2 localization in the NCE fraction correlated to PAB severity, we assessed the
352 relative ROR2 knockdown in NCD and NCE fractions and found PAB^{shRor2} had ~50% lower NCE
353 and ~25% lower NCD ROR2 in the RV (**Fig. 7i/j**). Strikingly, PAB^{shRor2} mice demonstrated less
354 severe RV dilation, decreased incidence of tricuspid insufficiency, better RV systolic function
355 measured by TAPSE (**Fig. 7j-l**), improved diastolic function by e' (**Fig. 7m**), less RV fibrosis,
356 and reduction in RV wall area by histology (**Fig. 7k-p** and **Supplementary Table 6**). ROR2
357 knockdown also ameliorated the proteostatic dysfunction in PAB with decreases in protein
358 synthesis, HSP70, and K48-linked ubiquitin without affecting proteasome capacity (**Fig. 7q-t**),
359 partially reversing the PAB-induced defects. Taken together, these data demonstrate that ROR2
360 knockdown protects from pathologic RV remodeling and improves RV function in response to
361 pressure overload, concomitant with partial reversion of altered proteostasis.

362

363 <u>ROR2 expression in human RVF correlates to proteasome capacity</u>

364 Finally, we sought to determine in human RVF the relationship between ROR2 and
365 proteostasis. To do so, we leveraged a collection of RV tissue obtained from non-failing organ
366 donors compared to DCM RVs collected at transplant. DCM RVs were stratified by having
367 preserved RV function versus RVF, and RVF hearts were further stratified by the level of NCD
368 and NCE ROR2. We evaluated for demographic, clinical, and anthropometric balance across all
369 relevant comparisons (**Fig 8a** and **Supplementary Tables 7-10**). We observed that high ROR2
370 expressing RVF, stratified by NCE or NCD fractions, demonstrated significantly increased
371 proteasome capacity at 0, 3.5, and 7 μM ATP (**Fig 8, Supplementary Fig 6a**, and
372 **Supplementary Table 11**; $p<0.05$). Interestingly, NCE ROR2 showed significant Pearson
373 correlation to proteasome capacity at each of the tested ATP levels ($r=0.68 – 0.82$, $p\leq 0.0008$;
374 **Fig 8c** and **Supplementary Tables 12**), whereas NCD ROR2 showed no clear relationship. We
375 also assessed the abundance of other proteostatic markers and found that high NCE ROR2
376 associated with a trend for decreased NCE HSP70 and that high NCD ROR2 associated with
377 increased NCD K48 ubiquitin (**Supplemental Fig 6b-e**). However, we found no clear patterns
378 for PSMB5 and total ubiquitin (**Supplemental Figure 6f-i)**. We conclude that in human
379 cardiomyopathy, as in mice, high ROR2 expression—particularly NCE ROR2—is associated
380 with an increase in proteasome capacity.

381

382 **Discussion**

383 RVF remains a widespread, challenging problem for which there are no proven therapies.[14] The
384 breadth of LVF medications have not shown clear benefit for RVF, indicating the presence of
385 distinct RVF mechanisms.[7-13,34] In severe human RVF, we found that the developmentally
386 restricted noncanonical WNT receptor ROR2 is pathologically reactivated by both
387 cardiomyocytes and fibroblasts.[16] We now find this expression pattern is recapitulated in mouse

388 pressure overload RVF, which contrasts with a prior report in mouse LVF for which induced
389 ROR2 is restricted to noncardiomyocytes.[29] Using NRVMs, in vivo murine models, and human
390 heart biospecimens, we now reveal a previously unrecognized role for ROR2 regulating
391 cardiomyocyte proteostasis with implications on contractile function and structure. Interestingly,
392 in mouse and human RVF, NCE localizing ROR2 demonstrates a stronger association than
393 NCD ROR2 with pathologic RV remodeling and proteostatic disruption. Our data point to a
394 model wherein ROR2 promotes protein synthesis without sufficient folding capacity (**Fig. 8d**).
395 Although UPS-mediated clearance is upregulated in this setting, this is either not sufficient to
396 meet the demands or, potentially, chronically maladaptive and ultimately converges on
397 cardiomyocyte functional compromise. Thus, we propose that addressing ROR2-mediated
398 proteostatic disruption represents a potential novel therapeutic avenue for RVF, for which no
399 proven therapies currently exist.

400

401 ROR2 is a noncanonical cell surface WNT receptor pseudokinase that signals through at least
402 three broad pathways: RAC/RHO regulation of cell polarity, activation of a JNK/cJUN
403 phosphorylation cascade, and activation of Ca^{2+}-responsive targets (e.g. PKC, CAMKII).[35] The
404 molecular and functional impact of pathogenic ROR2 has been best studied in cancer, for which
405 ROR2 causes context-specific pleiotropic phenotypes with mixed impact on cancer cell death,
406 invasion, and metastasis resulting in both positive and negative associations with patient
407 mortality.[36,37] Little is known about the role of ROR2 in cardiac pathology, but upregulation of
408 ROR2 leading to proteostatic disruption in RVF fits within the well-recognized paradigm of fetal
409 gene program reactivation during heart failure.[38,39] As the first functional organ, proliferating fetal
410 cardiomyocytes must maintain a high quality pool of contractile proteins, including some of the
411 largest in the proteome (e.g. Titin, Obscurin, Dystrophin, etc.), which is energetically demanding
412 and requires high protein synthesis matched to a robust folding capacity.[40-42] During human

413 heart development, *ROR2* and *HSPA1A/B* (HSP70) mRNA levels are positively correlated and
414 taper during later prenatal stages, consistent with amplified but balanced proteostasis of the
415 immature heart.[43] Postnatally, in mice we found age-dependent reductions in ventricular HSP70
416 and ROR2, with reductions in ROR2 preceding HSP70. In mouse PAB RV, translation, folding,
417 and proteasome capacity are all increased, but the presence of ubiquitin accumulation suggests
418 there is imbalance in these three components that favors excess translation.[42] Moreover, given
419 that ROR2 knockdown in PAB improves RV remodeling and function while most substantially
420 affecting protein synthesis, attenuating the translational hyperactivation of RVF may be the
421 critical factor to restore proteostatic balance. Prior work has shown that slowing translation with
422 rapamycin can improve translational fidelity in mTOR activated embryonic fibroblasts and can
423 rescue multiple preclinical LVF models.[44-46] In kind, rapamycin was shown to abrogate PAB-
424 induced RV hypertrophy and contractile dysfunction in rats.[44] Although protein translation and
425 UPS capacity were not measured, rapamycin did further increase PAB-induced ubiquitin
426 accumulation suggesting a decrease in UPS-mediated clearance, which may be the result of
427 slowing translation leading to improved overall proteome quality.

428

429 Proteostatic disruption is strongly implicated in heart failure, and its role in RVF is increasingly
430 recognized, yet developing targeted therapies has remained elusive.[47-49] Restoring proteostatic
431 balance would require precise control of synthesis, folding, and turnover, or a more practical
432 strategy of eliminating a pathogenic upstream regulator. Before this study, few links connected
433 ROR2—or noncanonical WNT signaling more broadly—to proteostasis. In cultured ovarian
434 carcinoma cells that typically express low ROR2, adenoviral ROR2 delivery activated the
435 unfolded protein response and triggered apoptosis.[50] These ROR2 effects in ovarian carcinoma
436 were rescued by blocking induction of the endoplasmic reticulum stress protein IRE1a. In
437 NRVMs, treatment with WNT5A—the only known ligand for ROR2—was shown to promote

438 protein synthesis and drive cardiomyocyte hypertrophy.[51,52] These WNT5A effects could be
439 blocked by preventing the membrane localization of the ROR2 binding partner VANGL2 or by
440 inhibiting JNK. Although JNK/cJUN are not classic regulators of protein synthesis, extensive
441 evidence shows crosstalk with mTOR and ERK. For example, both canonical and noncanonical
442 WNT activation can inhibit the signaling hub protein GSK3 through phosphorylation.[53,54]
443 Inhibiting GSK3 prevents it from phosphorylating several key substrates including β-catenin—
444 (leading to canonical WNT activation), TSC2 (activating mTORC1), and Raptor (suppressing
445 mTORC1).[55-57] JNK can also activate mTORC1 through Raptor phosphorylation, as observed in
446 HEK293 cells under osmotic stress.[58] ERK signaling provides an additional link. In A375
447 melanoma cells which have low endogenous ROR2, induction of ROR2 caused ERK
448 hyperactivation and cell death.[36] In isolated mouse cardiomyocytes, ERK1/2 activation and
449 HSP70 expression show reciprocal antagonism, and HSP70 knockdown was sufficient to cause
450 contractile and relaxation deficits similar to those we observed with $ROR2^{OE}$ NRVMs.[59] Thus,
451 ROR2 could lead to a pathologic increase in protein translation, thereby leading to proteostatic
452 disruption in cardiomyocytes, by activating mTOR or ERK signaling through modulating activity
453 of other true kinases (e.g. JNK/cJUN or GSK3)

454

455 Using orthogonal methods, we found that ROR2 can localize to the nucleus in the immature
456 heart and RVF. Nuclear enriched ROR2 in the NCE fraction strongly correlated to pathogenic
457 RV remodeling and proteostatic disruption. The functional role of nuclear ROR2 remains poorly
458 characterized, but in cancer nuclear ROR2 correlates to worse disease with increased
459 metastasis in melanoma and invasiveness in pancreatic cancer.[26,28] These pathophysiologic
460 associations with nuclear ROR2 underscore the importance of understanding the regulatory
461 mechanisms and functional roles (e.g. transcriptional modulation, scaffolding, etc.) of nuclear
462 localizing ROR2, which may further enable selective therapeutic targeting. For example,

463 ERK1/2 homeostatic and pathogenic roles are compartmentalized into the cytoplasm and
464 nucleus, respectively, and blocking its nuclear localization was shown to prevent pressure
465 induced cardiomyocyte hypertrophy and heart failure.[60,61]

466

467 **Limitations**

468 More work will be necessary to establish the therapeutic potential for targeting ROR2 in RVF.
469 While we have not observed sexual dimorphism for the impact of ROR2 in humans, we found
470 that overexpressing ROR2 in female mice led to a milder phenotype compared to males. This
471 sex difference in mice may fit with prior reports showing female mice are protected from
472 proteostatic disruption through higher basal chaperone expression and UPS capacity.[62-64] We
473 focused our in vitro mechanistic studies in cardiomyocytes, but ROR2 upregulation was also
474 observed in fibroblasts of human and mouse RVF. Importantly, in a prior mouse model of left
475 ventricular pressure overload where ROR2 induction was restricted to fibroblasts and
476 leukocytes, inducible total body combined ROR1/ROR2 knockout was lethal, diminished early
477 myofibroblast activation, and increased the abundance of inflammatory cells in the LV.[29] The
478 differences between that study and ours may be due to multiple factors including ubiquitous
479 knockout of both genes compared to knockdown of only ROR2 and by differences in the models
480 (RV vs LV pressure overload and the implicated cell populations) that may alter the impact of
481 loss of ROR2. Since ROR2 is known to be pleiotropic, understanding the role of ROR2 across
482 the spectrum of fibroblast activation states could have significant implications for its therapeutic
483 targetability.[29, 65] Finally, our analysis on the relationship between ROR2, RVF, and
484 proteostasis in humans reflects a single, uncontrolled timepoint which prevents us from
485 measuring dynamic processes (e.g. UPS flux, protein synthesis rates) that would more fully
486 capture this relationship.

487

488 **Conclusions**

489 In summary, we find compelling evidence to implicate ROR2 in RVF pathogenesis. Pathologic
490 reactivation of ROR2 causes proteostatic disruption in the RV, leading to RVF. In humans,
491 ROR2 is otherwise broadly absent from healthy mature tissues with its only other well
492 recognized induction occurring in cancer.[23] Thus, we conclude that targeting ROR2 offers a
493 potential therapeutic strategy to restore proteostatic balance and treat RVF, for which no
494 specific therapies currently exist.

495 **Acknowledgements**

496 We thank Julian Mintseris, Rachel Rodrigues, and Jonathan Van Vraken at Thermo Fisher
497 Scientific Center for Multiplexed Proteomics at Harvard Medical School for support in performing
498 proteomics. We thank the Day Lab at University of Pennsylvania for kindly providing adenovirus
499 to express GFPμ. The mouse PAB and echocardiography were performed by the Rodent
500 Cardiovascular Phenotyping Core (RRID: SCR_022419) at the University of Pennsylvania
501 supported by the Penn Cardiovascular Institute and NIH S10OD016393. Figures were
502 generated with assistance of BioRender.

503

504 **Sources of Funding**

505 J.J.E and Z.A. was supported by the Children's Hospital of Philadelphia Frontier Program
506 "Advanced Cardiac Therapies for Heart Failure". J.J.E. was also supported by National Institute
507 of Health (NIH) K08HL159311 and Z.A. was also supported by NIH HL152446 and HL152446.
508 K.U. was supported by the NIH (T32 HL007843). B.P. was supported by the NIH R01 HL149891
509 and the Foundation Leducq Research Grant no. 20CVD01. C.S.C. was supported by
510 Department of the Army (HT94252310080) and the NIH R35 GM154896. Human heart tissues
511 were procured with funding support from multiple NIH grants to K.M.: R01 AG017022, R01
512 HL089847, and R01 HL105993, and R01 HL133080.

513

514 **Author Contributions**

515 H.H., J.J.E., and Z.A. developed the concept and designed the experiments. J.J.E, Z.A., and
516 B.L.P. supervised and funded the project. J.J.E., H.H., K.U., E.A.S., G.U., S.K., and S.W.

517 conducted NRVM experiments. J.J.E., H.H., D.E., and R.T.S. conducted NRVM
518 contractility/relaxation experiments. J.J.E and H.H. performed mouse experiments. J.J.E, T.D.,
519 and C.S.C. conducted luciferase refolding and ^{35}S-Met labeling assays. J.B. and Y.Y. performed
520 RNAseq analysis. L. Lai, J.G., and S.S. performed mouse surgeries and physiologic
521 characterization. K.C.B. and K.M. supported human heart tissue procurement and clinical
522 characterization. H.R. contributed to microscopy image analysis. L.Li performed tissue
523 histology. All authors contributed to the manuscript preparation and approved the final version of
524 the manuscript.

525

526 **Disclosures**

527 There are no relevant disclosures.

528

529 **Corresponding author**

530 Correspondence to Jonathan J. Edwards and Zoltan Arany.

531 **References**

532 1 Lampert, B. C. & Teuteberg, J. J. Right ventricular failure after left ventricular assist
533 devices. *J Heart Lung Transplant* **34**, 1123-1130 (2015).
534 https://doi.org/10.1016/j.healun.2015.06.015

535 2 Zakeri, R. & Mohammed, S. F. Epidemiology of Right Ventricular Dysfunction in Heart
536 Failure with Preserved Ejection Fraction. *Curr Heart Fail Rep* **12**, 295-301 (2015).
537 https://doi.org/10.1007/s11897-015-0267-3

538 3 Khairy, P. *et al.* Long-term survival, modes of death, and predictors of mortality in
539 patients with Fontan surgery. *Circulation* **117**, 85-92 (2008).
540 https://doi.org/10.1161/CIRCULATIONAHA.107.738559

541 4 Piran, S., Veldtman, G., Siu, S., Webb, G. D. & Liu, P. P. Heart failure and ventricular
542 dysfunction in patients with single or systemic right ventricles. *Circulation* **105**, 1189-
543 1194 (2002).

544 5 Campo, A. *et al.* Outcomes of hospitalisation for right heart failure in pulmonary arterial
545 hypertension. *Eur Respir J* **38**, 359-367 (2011).
546 https://doi.org/10.1183/09031936.00148310

547 6 D'Amario, D. *et al.* Eligibility for the 4 Pharmacological Pillars in Heart Failure With
548 Reduced Ejection Fraction at Discharge. *J Am Heart Assoc* **12**, e029071 (2023).
549 https://doi.org/10.1161/JAHA.122.029071

550 7 Babu-Narayan, S. V. *et al.* Randomised trial of ramipril in repaired tetralogy of Fallot and
551 pulmonary regurgitation: the APPROPRIATE study (Ace inhibitors for Potential
552 PRevention Of the deleterious effects of Pulmonary Regurgitation In Adults with repaired
553 TEtralogy of Fallot). *Int J Cardiol* **154**, 299-305 (2012).
554 https://doi.org/10.1016/j.ijcard.2010.09.057

555 8 Dos, L. *et al.* Eplerenone in systemic right ventricle: double blind randomized clinical
556 trial. The evedes study. *Int J Cardiol* **168**, 5167-5173 (2013).
557 https://doi.org/10.1016/j.ijcard.2013.07.163
558 9 Doughan, A. R., McConnell, M. E. & Book, W. M. Effect of beta blockers (carvedilol or
559 metoprolol XL) in patients with transposition of great arteries and dysfunction of the
560 systemic right ventricle. *Am J Cardiol* **99**, 704-706 (2007).
561 https://doi.org/10.1016/j.amjcard.2006.10.025
562 10 Shaddy, R. E. *et al.* Carvedilol for children and adolescents with heart failure: a
563 randomized controlled trial. *JAMA* **298**, 1171-1179 (2007).
564 https://doi.org/10.1001/jama.298.10.1171
565 11 Bokma, J. P. *et al.* Effect of Losartan on Right Ventricular Dysfunction: Results From the
566 Double-Blind, Randomized REDEFINE Trial (Right Ventricular Dysfunction in Tetralogy
567 of Fallot: Inhibition of the Renin-Angiotensin-Aldosterone System) in Adults With
568 Repaired Tetralogy of Fallot. *Circulation* **137**, 1463-1471 (2018).
569 https://doi.org/10.1161/CIRCULATIONAHA.117.031438
570 12 Roche, S. L. & Redington, A. N. Right ventricle: wrong targets? Another blow for
571 pharmacotherapy in congenital heart diseases. *Circulation* **127**, 314-316 (2013).
572 https://doi.org/10.1161/CIRCULATIONAHA.112.155887
573 13 Hartupee, J. & Mann, D. L. Neurohormonal activation in heart failure with reduced
574 ejection fraction. *Nat Rev Cardiol* **14**, 30-38 (2017).
575 https://doi.org/10.1038/nrcardio.2016.163
576 14 Houston, B. A., Brittain, E. L. & Tedford, R. J. Right Ventricular Failure. *N Engl J Med*
577 **388**, 1111-1125 (2023). https://doi.org/10.1056/NEJMra2207410
578 15 Jurida, L. *et al.* A common gene signature of the right ventricle in failing rat and human
579 hearts. *Nat Cardiovasc Res* **3**, 819-840 (2024). https://doi.org/10.1038/s44161-024-
580 00485-1

581 16 Edwards, J. J. *et al.* Noncanonical WNT Activation in Human Right Ventricular Heart
582 Failure. *Front Cardiovasc Med* **7**, 582407 (2020).
583 https://doi.org/10.3389/fcvm.2020.582407
584 17 Takeuchi, S. *et al.* Mouse Ror2 receptor tyrosine kinase is required for the heart
585 development and limb formation. *Genes Cells* **5**, 71-78 (2000).
586 18 Guo, R. & Xing, Q. S. Roles of Wnt Signaling Pathway and ROR2 Receptor in
587 Embryonic Development: An Update Review Article. *Epigenet Insights* **15**,
588 25168657211064232 (2022). https://doi.org/10.1177/25168657211064232
589 19 Nomi, M. *et al.* Loss of mRor1 enhances the heart and skeletal abnormalities in mRor2-
590 deficient mice: redundant and pleiotropic functions of mRor1 and mRor2 receptor
591 tyrosine kinases. *Mol Cell Biol* **21**, 8329-8335 (2001).
592 https://doi.org/10.1128/MCB.21.24.8329-8335.2001
593 20 Perez-Riverol, Y. *et al.* The PRIDE database at 20 years: 2025 update. *Nucleic Acids*
594 *Res* **53**, D543-D553 (2025). https://doi.org/10.1093/nar/gkae1011
595 21 Scarborough, E. A. *et al.* Microtubules orchestrate local translation to enable cardiac
596 growth. *Nat Commun* **12**, 1547 (2021). https://doi.org/10.1038/s41467-021-21685-4
597 22 Chen, C. Y. *et al.* Suppression of detyrosinated microtubules improves cardiomyocyte
598 function in human heart failure. *Nat Med* **24**, 1225-1233 (2018).
599 https://doi.org/10.1038/s41591-018-0046-2
600 23 Morioka, K. *et al.* Orphan receptor tyrosine kinase ROR2 as a potential therapeutic
601 target for osteosarcoma. *Cancer Sci* **100**, 1227-1233 (2009).
602 https://doi.org/10.1111/j.1349-7006.2009.01165.x
603 24 Chaffin, M. *et al.* Single-nucleus profiling of human dilated and hypertrophic
604 cardiomyopathy. *Nature* **608**, 174-180 (2022). https://doi.org/10.1038/s41586-022-
605 04817-8

606 25 Litvinukova, M. *et al.* Cells of the adult human heart. *Nature* **588**, 466-472 (2020).
607 https://doi.org/10.1038/s41586-020-2797-4
608 26 Carbone, C. *et al.* Adipocytes sustain pancreatic cancer progression through a non-
609 canonical WNT paracrine network inducing ROR2 nuclear shuttling. *Int J Obes (Lond)*
610 **42**, 334-343 (2018). https://doi.org/10.1038/ijo.2017.285
611 27 Lopez-Bergami, P. ROR2, a driver of "phenotype switching" in melanoma? *Cancer Cell*
612 *Int* **22**, 288 (2022). https://doi.org/10.1186/s12935-022-02711-x
613 28 O'Connell, M. P. *et al.* The orphan tyrosine kinase receptor, ROR2, mediates Wnt5A
614 signaling in metastatic melanoma. *Oncogene* **29**, 34-44 (2010).
615 https://doi.org/10.1038/onc.2009.305
616 29 Chavkin, N. W. *et al.* The Cell Surface Receptors Ror1/2 Control Cardiac Myofibroblast
617 Differentiation. *J Am Heart Assoc* **10**, e019904 (2021).
618 https://doi.org/10.1161/JAHA.120.019904
619 30 Mandal, A. K. *et al.* Hsp110 chaperones control client fate determination in the hsp70-
620 Hsp90 chaperone system. *Mol Biol Cell* **21**, 1439-1448 (2010).
621 https://doi.org/10.1091/mbc.e09-09-0779
622 31 Schwanhausser, B. *et al.* Global quantification of mammalian gene expression control.
623 *Nature* **473**, 337-342 (2011). https://doi.org/10.1038/nature10098
624 32 Konopelski Snavely, S. E. *et al.* Proteomic analysis identifies the E3 ubiquitin ligase
625 Pdzrn3 as a regulatory target of Wnt5a-Ror signaling. *Proc Natl Acad Sci U S A* **118**
626 (2021). https://doi.org/10.1073/pnas.2104944118
627 33 Pernot, M. *et al.* Decrease of Pdzrn3 is required for heart maturation and protects
628 against heart failure. *Sci Rep* **12**, 8 (2022). https://doi.org/10.1038/s41598-021-03795-7
629 34 Jurida, L. *et al.* A common gene signature of the right ventricle in failing rat and human
630 hearts. *Nature Cardiovascular Research* **3**, 819-840 (2024).
631 https://doi.org/10.1038/s44161-024-00485-1

632 35 Debebe, Z. & Rathmell, W. K. Ror2 as a therapeutic target in cancer. *Pharmacol Ther*
633 **150**, 143-148 (2015). https://doi.org/10.1016/j.pharmthera.2015.01.010
634 36 Castro, M. V. & Lopez-Bergami, P. Cellular and molecular mechanisms implicated in the
635 dual role of ROR2 in cancer. *Crit Rev Oncol Hematol* **170**, 103595 (2022).
636 https://doi.org/10.1016/j.critrevonc.2022.103595
637 37 Ford, C. E., Qian Ma, S. S., Quadir, A. & Ward, R. L. The dual role of the novel Wnt
638 receptor tyrosine kinase, ROR2, in human carcinogenesis. *Int J Cancer* **133**, 779-787
639 (2013). https://doi.org/10.1002/ijc.27984
640 38 van der Pol, A., Hoes, M. F., de Boer, R. A. & van der Meer, P. Cardiac foetal
641 reprogramming: a tool to exploit novel treatment targets for the failing heart. *J Intern Med*
642 **288**, 491-506 (2020). https://doi.org/10.1111/joim.13094
643 39 Poon, E. *et al.* Proteomic Analysis of Human Pluripotent Stem Cell-Derived, Fetal, and
644 Adult Ventricular Cardiomyocytes Reveals Pathways Crucial for Cardiac Metabolism and
645 Maturation. *Circ Cardiovasc Genet* **8**, 427-436 (2015).
646 https://doi.org/10.1161/CIRCGENETICS.114.000918
647 40 Kotter, S. & Kruger, M. Protein Quality Control at the Sarcomere: Titin Protection and
648 Turnover and Implications for Disease Development. *Front Physiol* **13**, 914296 (2022).
649 https://doi.org/10.3389/fphys.2022.914296
650 41 Nagai, R., Low, R. B., Stirewalt, W. S., Alpert, N. R. & Litten, R. Z. Efficiency and
651 capacity of protein synthesis are increased in pressure overload cardiac hypertrophy.
652 *Am J Physiol* **255**, H325-328 (1988). https://doi.org/10.1152/ajpheart.1988.255.2.H325
653 42 Lewis, Y. E. *et al.* Localization of transcripts, translation, and degradation for
654 spatiotemporal sarcomere maintenance. *J Mol Cell Cardiol* **116**, 16-28 (2018).
655 https://doi.org/10.1016/j.yjmcc.2018.01.012

656 43 Pervolaraki, E., Dachtler, J., Anderson, R. A. & Holden, A. V. The developmental
657 transcriptome of the human heart. *Sci Rep* **8**, 15362 (2018).
658 https://doi.org/10.1038/s41598-018-33837-6
659 44 Harston, R. K. *et al.* Rapamycin treatment augments both protein ubiquitination and Akt
660 activation in pressure-overloaded rat myocardium. *Am J Physiol Heart Circ Physiol* **300**,
661 H1696-1706 (2011). https://doi.org/10.1152/ajpheart.00545.2010
662 45 Fleming, N. D., Samsa, L. A., Hassel, D., Qian, L. & Liu, J. Rapamycin attenuates
663 pathological hypertrophy caused by an absence of trabecular formation. *Sci Rep* **8**, 8584
664 (2018). https://doi.org/10.1038/s41598-018-26843-1
665 46 Li, S. *et al.* Mechanism of Eccentric Cardiomyocyte Hypertrophy Secondary to Severe
666 Mitral Regurgitation. *Circulation* **141**, 1787-1799 (2020).
667 https://doi.org/10.1161/CIRCULATIONAHA.119.043939
668 47 Buhringer, H., Doroudgar, S., Wang, X., Frey, N. & Rangrez, A. Y. Editorial: Proteostasis
669 in cardiac health and disease. *Front Mol Biosci* **11**, 1433721 (2024).
670 https://doi.org/10.3389/fmolb.2024.1433721
671 48 Heitmeier, T. *et al.* Altered proteasome function in right ventricular hypertrophy.
672 *Cardiovasc Res* **116**, 406-415 (2020). https://doi.org/10.1093/cvr/cvz103
673 49 Rajagopalan, V. *et al.* Altered ubiquitin-proteasome signaling in right ventricular
674 hypertrophy and failure. *Am J Physiol Heart Circ Physiol* **305**, H551-562 (2013).
675 https://doi.org/10.1152/ajpheart.00771.2012
676 50 Li, R. *et al.* ROR2 induces cell apoptosis via activating IRE1alpha/JNK/CHOP pathway
677 in high-grade serous ovarian carcinoma in vitro and in vivo. *J Transl Med* **17**, 428 (2019).
678 https://doi.org/10.1186/s12967-019-02178-x
679 51 Hagenmueller, M. *et al.* Dapper-1 is essential for Wnt5a induced cardiomyocyte
680 hypertrophy by regulating the Wnt/PCP pathway. *FEBS Lett* **588**, 2230-2237 (2014).
681 https://doi.org/10.1016/j.febslet.2014.05.039

682 52 Zhang, P. *et al.* Vangl2 is essential for myocardial remodeling activated by Wnt/JNK
683 signaling. *Exp Cell Res* **365**, 33-45 (2018). https://doi.org/10.1016/j.yexcr.2018.02.012
684 53 Landin Malt, A. *et al.* Non-Canonical Wnt Signaling Regulates Cochlear Outgrowth and
685 Planar Cell Polarity via Gsk3beta Inhibition. *Front Cell Dev Biol* **9**, 649830 (2021).
686 https://doi.org/10.3389/fcell.2021.649830
687 54 Wu, D. & Pan, W. GSK3: a multifaceted kinase in Wnt signaling. *Trends Biochem Sci* **35**,
688 161-168 (2010). https://doi.org/10.1016/j.tibs.2009.10.002
689 55 Zhai, P., Sciarretta, S., Galeotti, J., Volpe, M. & Sadoshima, J. Differential roles of GSK-
690 3beta during myocardial ischemia and ischemia/reperfusion. *Circ Res* **109**, 502-511
691 (2011). https://doi.org/10.1161/CIRCRESAHA.111.249532
692 56 Stretton, C. *et al.* GSK3-mediated raptor phosphorylation supports amino-acid-
693 dependent mTORC1-directed signalling. *Biochem J* **470**, 207-221 (2015).
694 https://doi.org/10.1042/BJ20150404
695 57 Robertson, H., Hayes, J. D. & Sutherland, C. A partnership with the proteasome; the
696 destructive nature of GSK3. *Biochem Pharmacol* **147**, 77-92 (2018).
697 https://doi.org/10.1016/j.bcp.2017.10.016
698 58 Kwak, D. *et al.* Osmotic stress regulates mammalian target of rapamycin (mTOR)
699 complex 1 via c-Jun N-terminal Kinase (JNK)-mediated Raptor protein phosphorylation.
700 *J Biol Chem* **287**, 18398-18407 (2012). https://doi.org/10.1074/jbc.M111.326538
701 59 Kim, Y. K. *et al.* Deletion of the inducible 70-kDa heat shock protein genes in mice
702 impairs cardiac contractile function and calcium handling associated with hypertrophy.
703 *Circulation* **113**, 2589-2597 (2006).
704 https://doi.org/10.1161/CIRCULATIONAHA.105.598409
705 60 Lorenz, K., Schmitt, J. P., Schmitteckert, E. M. & Lohse, M. J. A new type of ERK1/2
706 autophosphorylation causes cardiac hypertrophy. *Nat Med* **15**, 75-83 (2009).
707 https://doi.org/10.1038/nm.1893

708 61 Tomasovic, A. *et al.* Interference with ERK-dimerization at the nucleocytosolic interface
709 targets pathological ERK1/2 signaling without cardiotoxic side-effects. *Nat Commun* **11**,
710 1733 (2020). https://doi.org/10.1038/s41467-020-15505-4
711 62 Karagias, G. *et al.* Transcriptome characterization of estrogen-treated human
712 myocardium identifies myosin regulatory light chain interacting protein as a sex-specific
713 element influencing contractile function. *J Am Coll Cardiol* **59**, 410-417 (2012).
714 https://doi.org/10.1016/j.jacc.2011.09.054
715 63 Olazabal, U. E., Pfaff, D. W. & Mobbs, C. V. Sex differences in the regulation of heat
716 shock protein 70 kDa and 90 kDa in the rat ventromedial hypothalamus by estrogen.
717 *Brain Res* **596**, 311-314 (1992). https://doi.org/10.1016/0006-8993(92)91563-t
718 64 Voss, M. R. *et al.* Gender differences in the expression of heat shock proteins: the effect
719 of estrogen. *Am J Physiol Heart Circ Physiol* **285**, H687-692 (2003).
720 https://doi.org/10.1152/ajpheart.01000.2002
721 65 Mitra, A. *et al.* LOSS OF ROR2 TYROSINE KINASE RECEPTOR IS ASSOCIATED
722 WITH ENDOTHELIAL DYSFUNCTION IN PAH VIA INAPPROPRIATE INTEGRIN β1
723 ACTIVATION. *bioRxiv*, 2025.2004.2028.651135 (2025).
724 https://doi.org/10.1101/2025.04.28.651135
725 66 Medvar, B., Raghuram, V., Pisitkun, T., Sarkar, A. & Knepper, M. A. Comprehensive
726 database of human E3 ubiquitin ligases: application to aquaporin-2 regulation. *Physiol*
727 *Genomics* **48**, 502-512 (2016). https://doi.org/10.1152/physiolgenomics.00031.2016
728 67 Droste, P. *et al.* Semiautomated pipeline for quantitative analysis of heart
729 histopathology. *J Transl Med* **21**, 666 (2023). https://doi.org/10.1186/s12967-023-04544-
730 2
731 68 McAfee, Q. *et al.* Truncated titin proteins in dilated cardiomyopathy. *Sci Transl Med* **13**,
732 eabd7287 (2021). https://doi.org/10.1126/scitranslmed.abd7287

733 69 Rabkin, S. W., Lodha, P. & Kong, J. Y. Reduction of protein synthesis and statin-induced
734 cardiomyocyte cell death. *Cardiovasc Toxicol* **7**, 1-9 (2007).
735 https://doi.org/10.1007/s12012-007-0003-7
736 70 Powell, S. R., Davies, K. J. & Divald, A. Optimal determination of heart tissue 26S-
737 proteasome activity requires maximal stimulating ATP concentrations. *J Mol Cell Cardiol*
738 **42**, 265-269 (2007). https://doi.org/10.1016/j.yjmcc.2006.10.010
739 71 Conn, C. S. & Qian, S. B. Nutrient signaling in protein homeostasis: an increase in
740 quantity at the expense of quality. *Sci Signal* **6**, ra24 (2013).
741 https://doi.org/10.1126/scisignal.2003520
742 72 Navarrete-Perea, J., Yu, Q., Gygi, S. P. & Paulo, J. A. Streamlined Tandem Mass Tag
743 (SL-TMT) Protocol: An Efficient Strategy for Quantitative (Phospho)proteome Profiling
744 Using Tandem Mass Tag-Synchronous Precursor Selection-MS3. *J Proteome Res* **17**,
745 2226-2236 (2018). https://doi.org/10.1021/acs.jproteome.8b00217
746 73 Li, J. *et al.* TMTpro-18plex: The Expanded and Complete Set of TMTpro Reagents for
747 Sample Multiplexing. *J Proteome Res* **20**, 2964-2972 (2021).
748 https://doi.org/10.1021/acs.jproteome.1c00168
749 74 Schweppe, D. K. *et al.* Full-Featured, Real-Time Database Searching Platform Enables
750 Fast and Accurate Multiplexed Quantitative Proteomics. *J Proteome Res* **19**, 2026-2034
751 (2020). https://doi.org/10.1021/acs.jproteome.9b00860
752 75 Rad, R. *et al.* Improved Monoisotopic Mass Estimation for Deeper Proteome Coverage.
753 *J Proteome Res* **20**, 591-598 (2021). https://doi.org/10.1021/acs.jproteome.0c00563
754
755

756 **Figures and Legends**

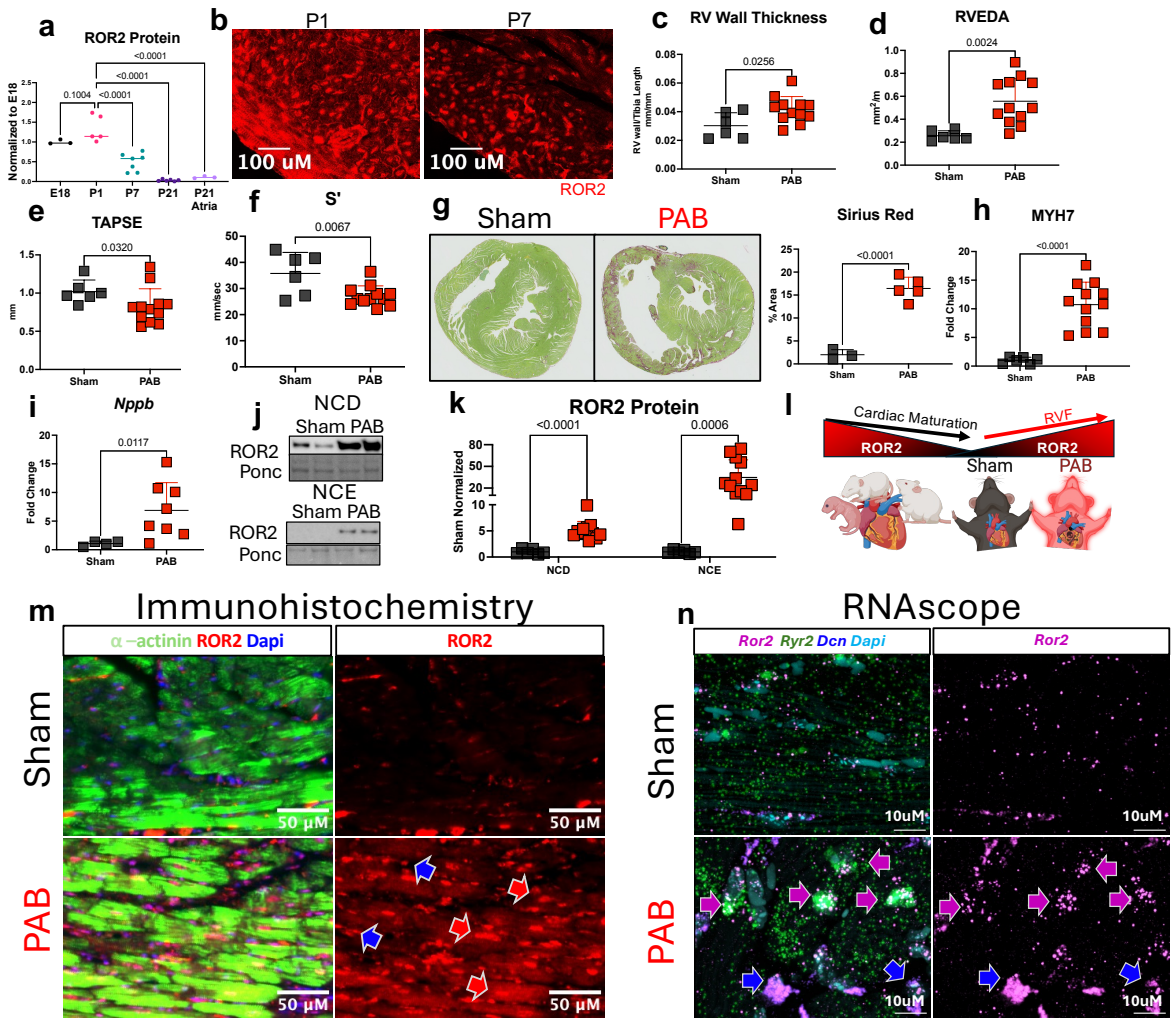

Fig. 1 ROR2 is a developmentally restricted protein that is robustly upregulated in RVF. (**a**) ROR2 protein expression was measured in the ventricular tissue using thiourea extraction by western from P2 to P21 and in P21 atria (N=3-7/age group; statistics by One-Way ANOVA with Two step FDR correction and T-test for P21 ventricle vs atria). (**b**) ROR2 immunohistochemistry was performed to evaluate localization, which is observed at the cell membrane and nucleus. (**c-f**) PAB was performed in 9-week-old C57BL/6J male mice with echocardiogram performed after 2 weeks to assess RV remodeling and systolic function, Sirius red staining to assess for fibrosis quantified using ImageJ **(g,** 10X magnification), western blot to assess induction of fetal MYH7 (**h**) and qPCR to assess expression *Nppb* in the RV free wall. Protein fractionation was performed to assess expression of ROR2 in the NCD (cytoplasmic, triton soluble) and the NCE

768 fractions (triton-insoluble) (**j-l**). ROR2 immunohistochemistry (**m**, 20X magnification) and
769 RNAscope (**n**, 63X magnification), was performed to assess cell type pattern of expression for
770 ROR2 induction in PAB using α-actinin and *Ryr2* to identify cardiomyocytes and *Dcn* to identify
771 fibroblasts in PAB RV. Statistics for PAB analyses by unpaired t-test or Mann-Whitney,
772 depending on normality (n= 3-6 for sham, n=5-12 for PAB).

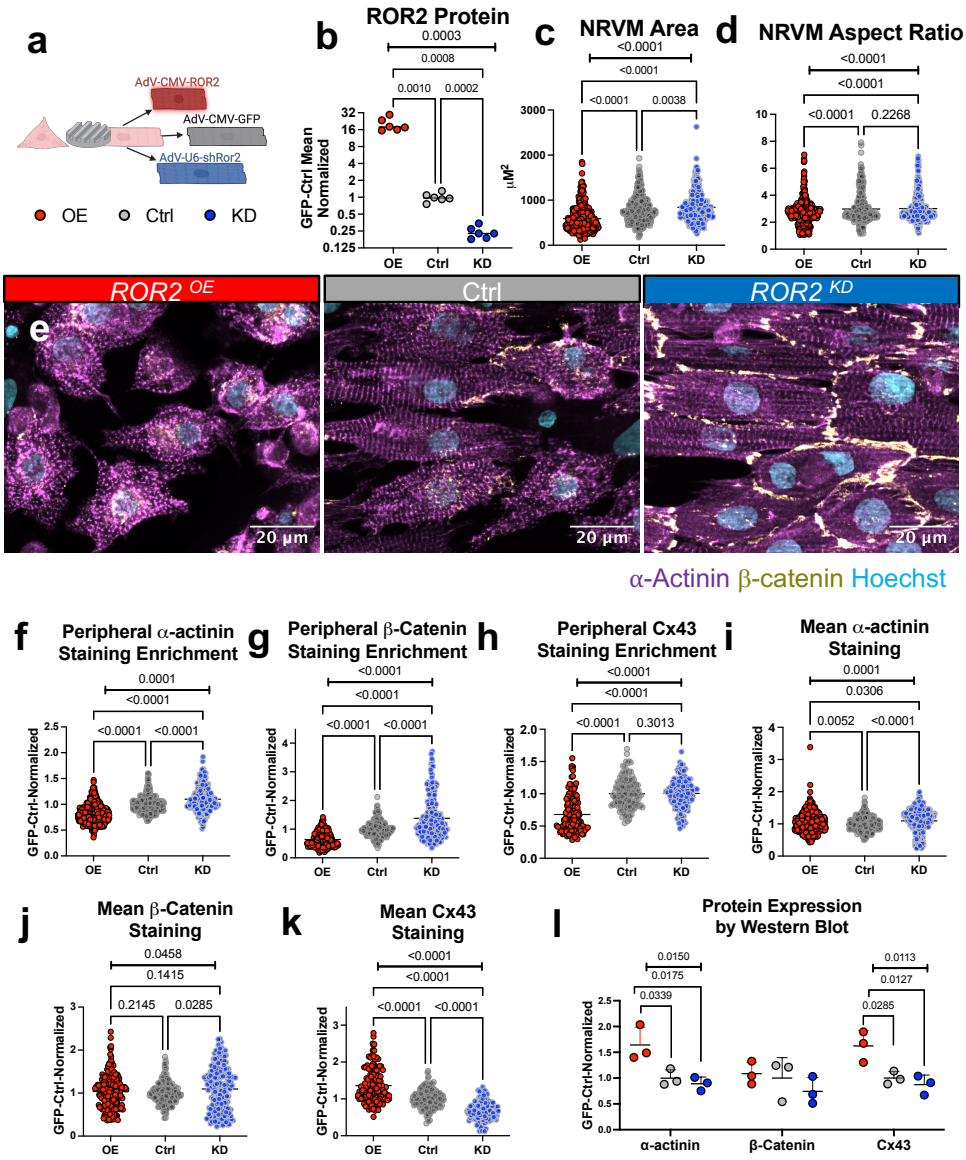

Fig. 2 ROR2 regulates in vitro cardiomyocyte morphology. (**a/b**) NRVMs were cultured on nanopatterned surface and received adenovirus to overexpress human ROR2, knockdown ROR2, or express GFP alone. NRVM structure was evaluated by Airyscan confocal microscopy (**c-e**, 63X magnification) using FIJI to generate maximum intensity projections and quantify cell size and aspect ratio (major/minor axis using the fit ellipse). (**f-k**) FIJI was used to quantify mean staining intensity; peripheral intensity enrichment was further measured as described in the methods by subtracting the inner cell integrated intensity (total area shrunken by 2μm) from the full cell integrated for α-actinin, β-catenin, and Cx43 (N=8-9 NRVM isolations, n= 341-411

782 cardiomyocytes/group). Total protein expression for these were also assessed by western blot

783 (n=3/group). One-Way ANOVA with two-stage step up Benjamini correction).

784

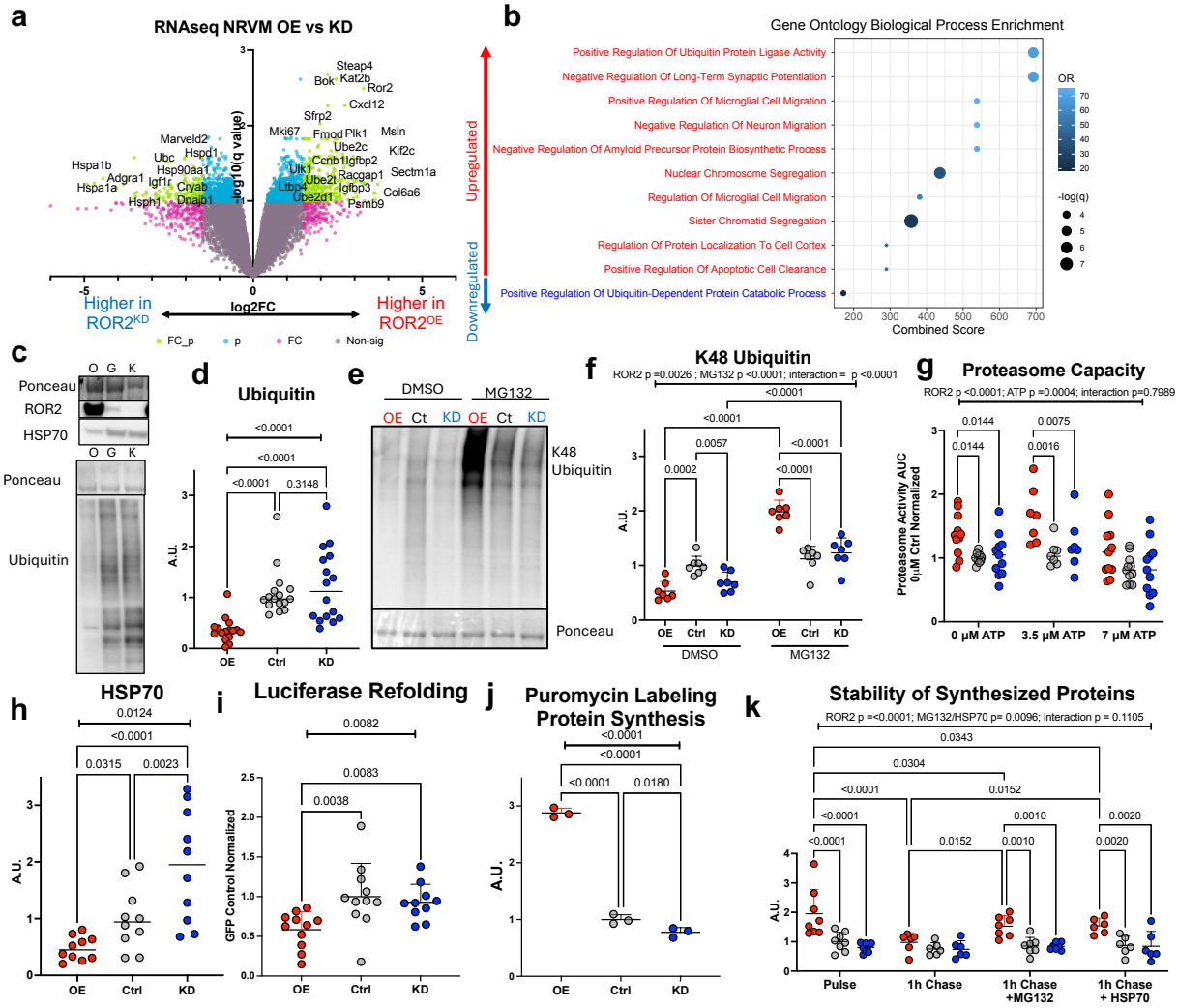

Fig. 3 ROR2 regulates in vitro cardiomyocyte proteostasis.

RNAseq with Voom/Limma was performed to assess differential gene expression between ROR2^{OE} and ROR2^{KD} NRVMs, with volcano plot (**a**) highlighting notable genes including transcriptional changes in the proteostatic pathways including folding (e.g. *Hspa1a/b, Hsph1, Cryab*) and pathway enrichment analysis (**b**) performed by Gene Ontology Biological Processes (n=4/group). Western blot was used to evaluate total ubiquitin (**c/d**, n=16/group) and HSP70 (**c/h**, n=10/group) between ROR2^{OE}, ROR2^{KD}, and controls. NRVMs were treated with 1μM MG132 or DMSO for 24 hours prior to collection to assess the flux of K48-linked ubiquitin clearance by the UPS (**e/f**, n=7/group). Proteasome capacity was measured using the chymotrypsin proteasome substrate Suc-LLVY-AMC with cell lysates in the absence or

796 presence of indicated supplemented ATP (**g**, n=7-11/group and ATP condition). Protein
797 refolding was measured using heat shocked luciferase (**i**, n=11/group), measured by
798 luminescence after addition of luciferin. Protein synthesis rates were measured using 0.55
799 μg/mL tyrosyl-tRNA analogue puromycin for 1 hour pulse with immediate collection (**j**) or with a
800 subsequent 1 hour chase (**k**) including cycloheximide (20 μg/mL) to block further translation with
801 or without MG132 (20 μM) or $HSP70^{OE}$ (n=6-8/group). Statistical comparisons were performed
802 with One-Way ANOVAs or Two-Way ANOVAs as indicated on graphs, with two-stage step up
803 Benjamini correction.

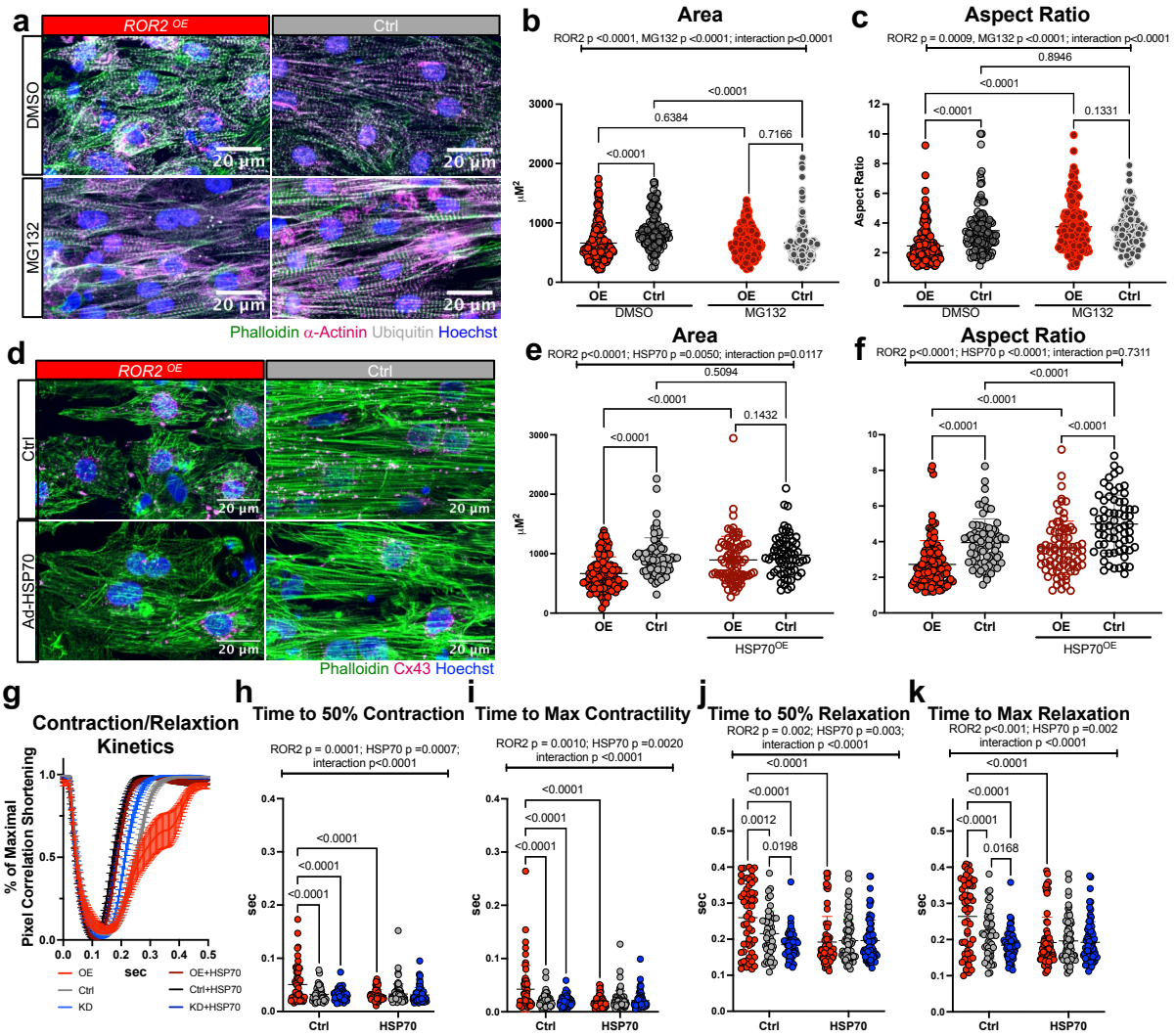

Fig 4. Proteostatic disruption is responsible for ROR2-mediated cardiomyocyte structural and functional defects

The impact of proteasome inhibition (**a-c**; MG132 1µM for 24 hours, n=129-183/group) and increased HSP70 expression (**d-f**; 24 hours of adenoviral expression of *Hspa1b***,** n=65-111/group) on ROR2^{OE}-mediated change in cell area and aspect ratio was evaluated as described above. Using a Cytocypher pacing apparatus, the impact of ROR2^{OE} and ROR2^{KD} on contractile and relaxation kinetics (**g-k**) were measured using CytoMotion Pixel Correlation with IonOptix software (n=48-75/group from three separate NRVM isolations). Statistics by Two Way ANOVA without correction (**a-f**) or with two-stage step up Benjamini correction (**i-l**).

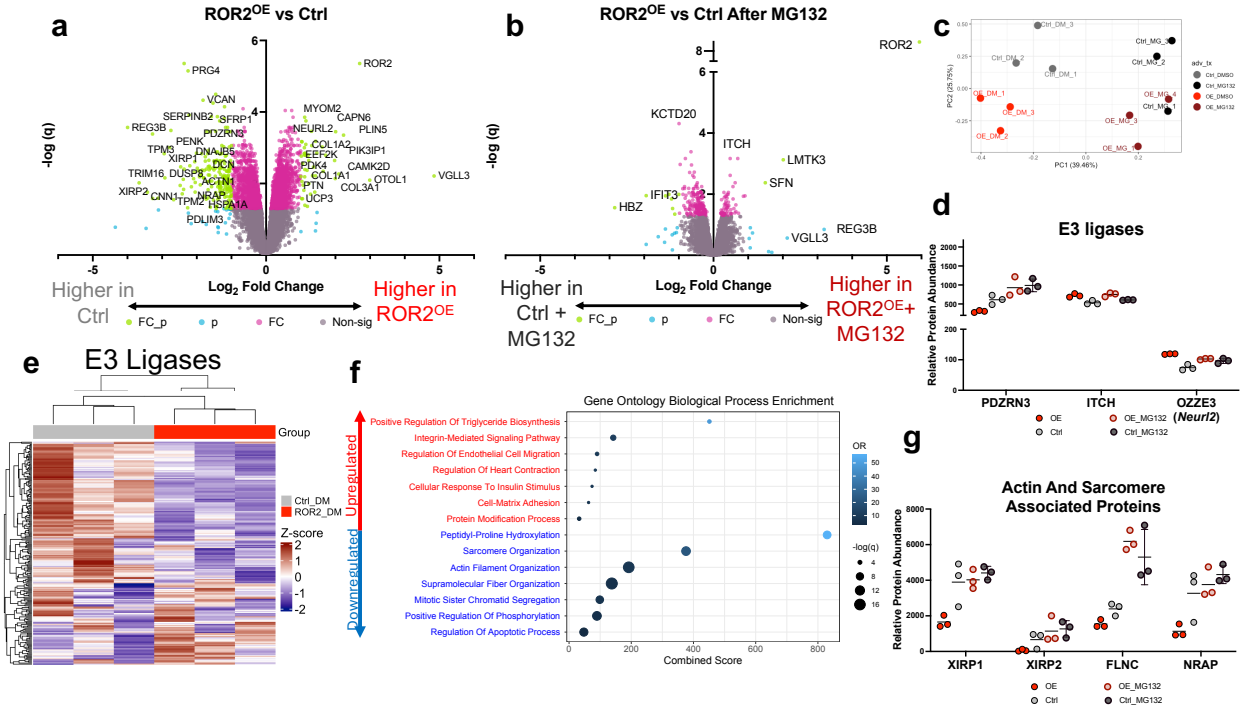

Fig. 5 ROR2 mediated proteostatic disruption impacts cardiomyocyte structural proteins

The interaction of ROR2^{OE} and proteasome inhibition on the impact of the NRVM proteome was investigated by TMT-labeled mass spectrometry-based proteomics using Voom/Limma to evaluate differential protein abundance, with visualization by volcano (**a/b**) and PCA plots (**c**). Normalized abundance of representative (**d**) E3 ligases is displayed by dotplot and heatmap (**e**) using a previously published comprehensive list of human E3 ligases.[66] (**d/e**) Differential protein abundance enrichment analysis was performed for GO Biological Processes (**f**). Representative change in actin and sarcomere associated proteins with ROR2^{OE} and MG132 are displayed by dotplot (**g**).

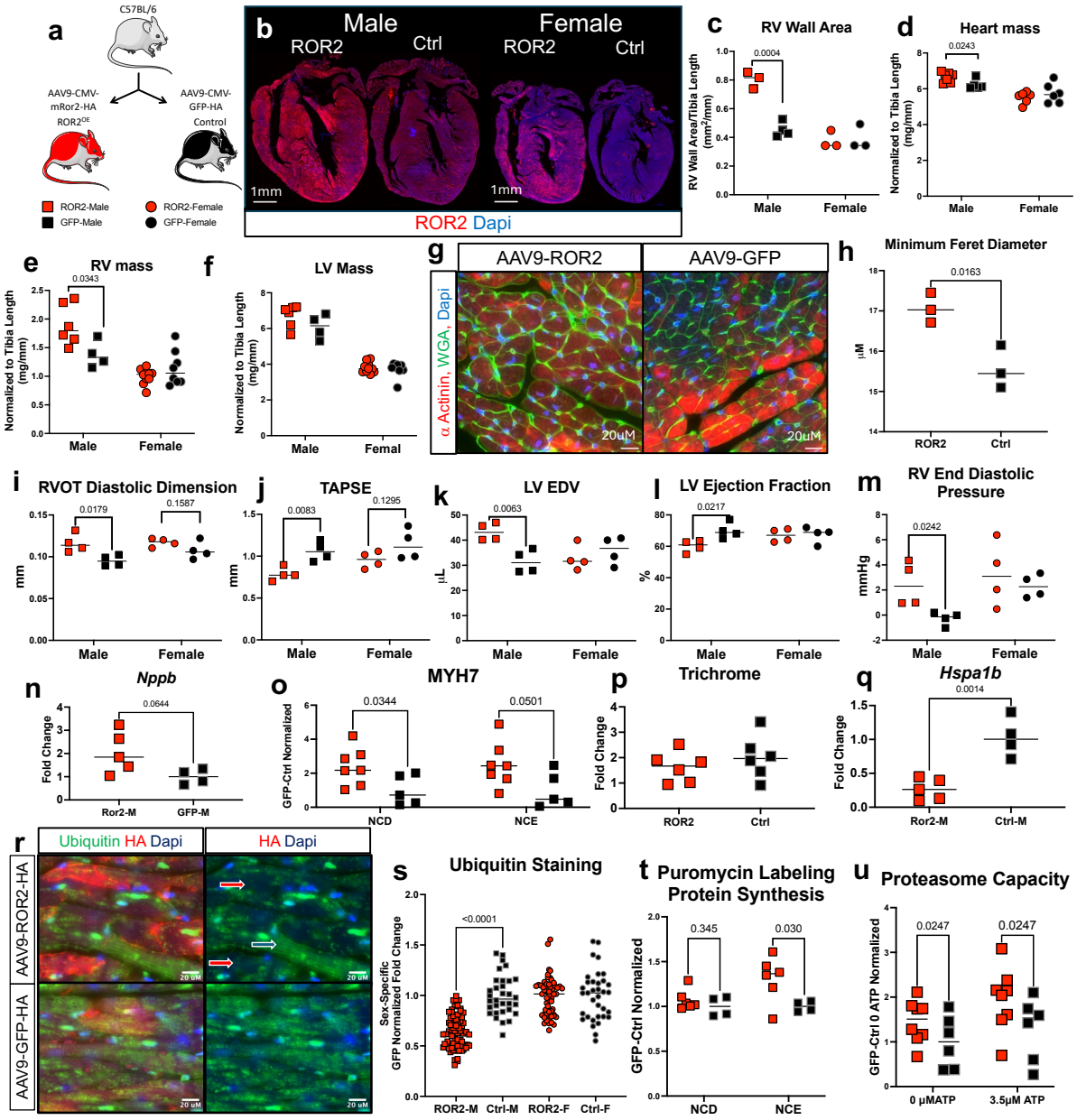

Fig. 6 Cardiac ROR2 induction is sufficient to cause RVF and proteostatic disruption in mice. (**a**) The impact of cardiac ROR2^{OE} was tested using AAV9 delivery of HA-tagged *Ror2* vs GFP in male and female mice at age 4 weeks with phenotyping performed at age 12 weeks. Cardiac ROR2^{OE} caused a male predominant phenotype with increase in RV wall area (**b** representative 10X magnification and **c**) quantified using FIJI with color deconvolution to identify epi and endocardial borders. Total heart mass after trimming great vessels and RV free wall and

832 LV mass were measure after removal of atria and separation of RV free wall (**d-f**). RV
833 cardiomyocyte cross sectional area was measured using HeartJ[67] FIJI package on WGA
834 stained section and quantifying the minimum Feret Diameter (**g/h**, 40X magnification).
835 Echocardiography was performed to assess biventricular size and systolic function (**i-l**) and
836 jugular catheterization was performed to assess RV end diastolic pressure (**m**). Expression of
837 *Nppb* was measured by qPCR (**n**) and fetal MYH7 was measured by western blot (**o**). Fibrosis
838 was measured using trichrome staining of RV free wall tissue (**p**). Proteostatic characterization
839 including assessment of *Hspa1b* by qPCR (**q**), ubiquitin immunohistochemistry of HA-tag (i.e.
840 AAV infected cardiomyocytes) (**r/s**, 60X magnification), puromycin labeling to measure protein
841 synthesis rates using a 1-hour puromycin pulses by intraperitoneal injection (**t**) and proteasome
842 capacity using Suc-LLVY-AMC (**u**). Statistical comparisons performed using t-test or Mann
843 Whitney depending on normality, (n=3-8 mice/group and 32-72 RV cardiomyocytes/group for
844 panel **s**).
845

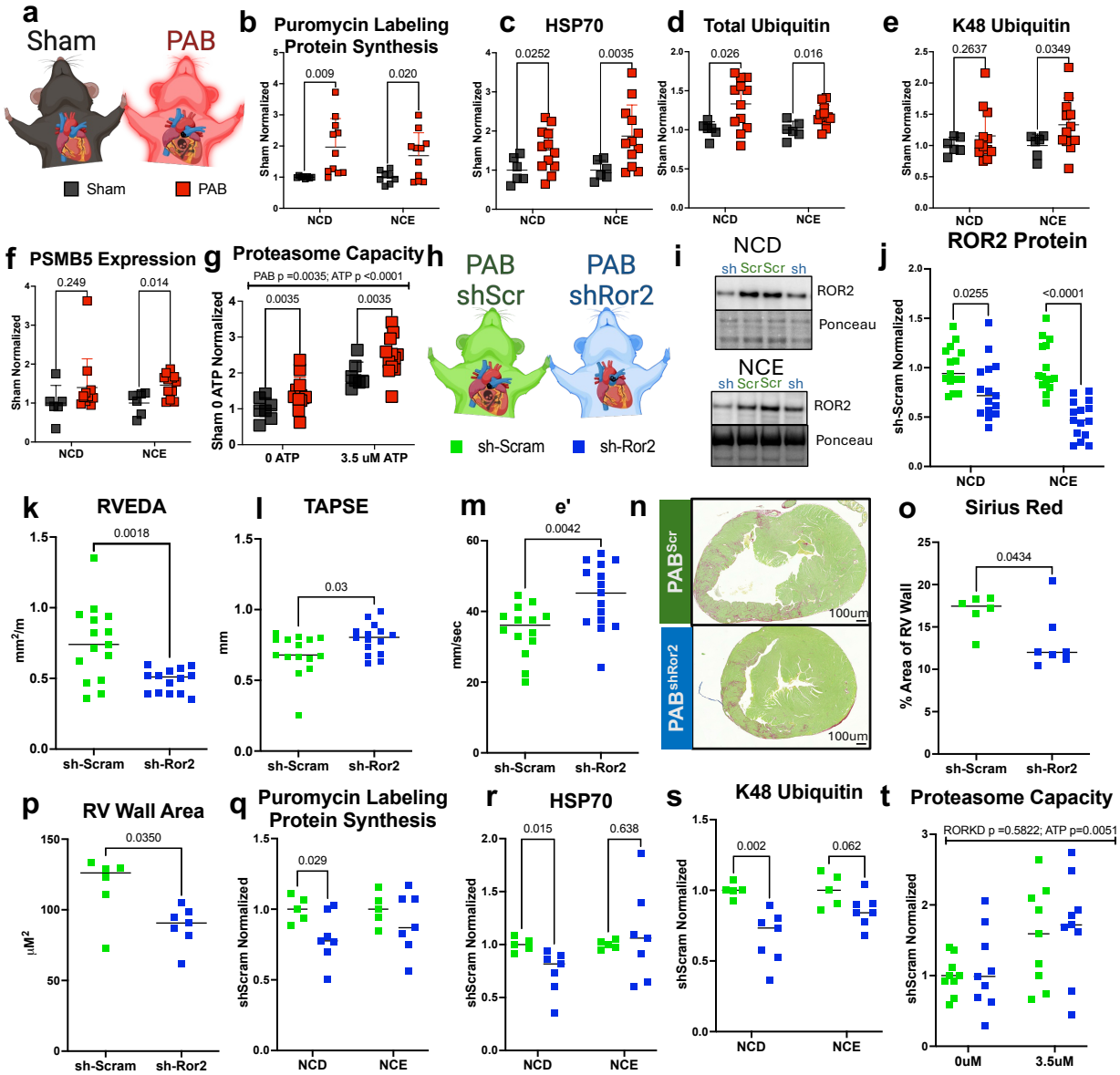

Fig. 7 ROR2 knockdown improves RVF and proteostatic burden in RV pressure overload. Proteostatic characterizations were performed for PAB and sham mice (**a**) by puromycin labeling to measure protein synthesis (**b**), expression of HSP70 (**c**), total ubiquitin (**d**), K48-linked ubiquitin (**e**), and PSMB5 expression (**f**) by western blot in NCD and NCE fractions. Proteasome capacity was measured using Suc LLVY-AMC (**g**). ROR2^{KD} was achieved by AAV9-delivery of *Ror2* targeting shRNA (PAB^{shRor2}) delivered by retroorbital injection 4-weeks

854 prior to PAB/sham, which reduced NCD (~25%) and NCE (~50%) ROR2 expression compared
855 to scrambled shRNA (PAB^{Scr}; **h-j**). Echocardiography was performed 2 weeks after PAB to
856 assess RV remodeling, systolic and diastolic function (**k-m**). Histology using Sirius red of RV
857 free wall and FIJI to assess RV area and fibrosis percent using colour deconvolution (**n-p**).
858 Proteostatic state in PAB^{shScr} compared to PAB^{shRor2} was characterized using puromycin
859 labeling, K48 ubiquitin and HSP70 expression, and proteasome capacity by Suc-LLVY-AMC as
860 above (**q-t**). Statistics by t-test or Mann Whitney depending on normality (n=6-7 for Sham vs
861 PAB n=9-12 and n=5-15 PAB^{shScr} vs n=7-14 for PAB^{shRor2}), or Two-Way ANOVA for proteasome
862 capacity.
863

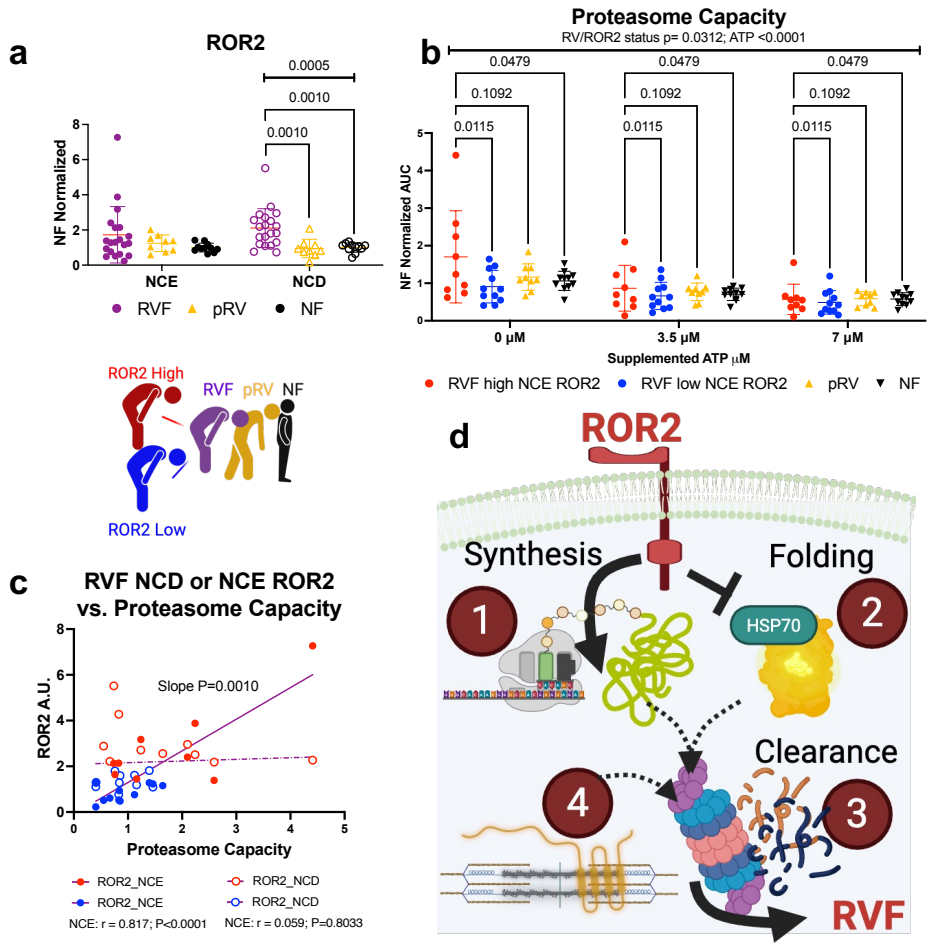

Fig. 8 ROR2 expression is associated with proteostatic disruption in human RVF. (**a**) ROR2 expression in NCE (filled in symbols) and NCD (open symbols) fractions was measured in the RVs from humans with RVF from dilated cardiomyopathy with (purple), preserved RV function (orange triangles, pRV), or nonfailing (NF, black). RVF samples were further stratified by high (red symbols) and low (blue symbols) NCE/NCD ROR2. (**b**) Proteasome capacity was compared across human RV functional groups. (**c**) Within RVF, NCD/NCE ROR2 levels were assessed for Pearson correlation against proteasome capacity (noted below graph) and for differences in linear slopes. Statistics by Kruskal-Wallis (**a**) or Two Way ANOVA (**b**) with two-stage step up Benjamini correction (n=9-11/group). (**d**) Taken together, our work reveals a model wherein high ROR2 expression in cardiomyocytes disrupts proteostasis with increased protein synthesis (1) and reduced folding (2) that results in a poor-quality proteome, leading

876 cardiomyocytes to clear proteins by the UPS (3), which disrupts cardiomyocyte structure and

877 function (4).